

3-4-2013

## Periodic Anderson model with electron-phonon correlated conduction band

Peng Zhang  
*Louisiana State University*

Peter Reis  
*Louisiana State University*

Ka Ming Tam  
*Louisiana State University*

Mark Jarrell  
*Louisiana State University*

Juana Moreno  
*Louisiana State University*

*See next page for additional authors*

Follow this and additional works at: [https://digitalcommons.lsu.edu/physics\\_astronomy\\_pubs](https://digitalcommons.lsu.edu/physics_astronomy_pubs)

---

### Recommended Citation

Zhang, P., Reis, P., Tam, K., Jarrell, M., Moreno, J., Assaad, F., & McMahan, A. (2013). Periodic Anderson model with electron-phonon correlated conduction band. *Physical Review B - Condensed Matter and Materials Physics*, 87 (12) <https://doi.org/10.1103/PhysRevB.87.121102>

This Article is brought to you for free and open access by the Department of Physics & Astronomy at LSU Digital Commons. It has been accepted for inclusion in Faculty Publications by an authorized administrator of LSU Digital Commons. For more information, please contact [ir@lsu.edu](mailto:ir@lsu.edu).

---

**Authors**

Peng Zhang, Peter Reis, Ka Ming Tam, Mark Jarrell, Juana Moreno, Fagher Assaad, and A. K. McMahan

# Periodic Anderson model with electron-phonon correlated conduction band

Peng Zhang,<sup>1</sup> Peter Reis,<sup>1</sup> Ka-Ming Tam,<sup>1</sup> Mark Jarrell,<sup>1</sup> Juana Moreno,<sup>1</sup> Fakher Assaad,<sup>2</sup> and Andy McMahan<sup>3</sup>

<sup>1</sup>*Department of Physics and Astronomy, Louisiana State University, Baton Rouge, Louisiana 70803, USA*

<sup>2</sup>*Institute for Theoretical Physics and Astrophysics, University of Würzburg, Germany*

<sup>3</sup>*Lawrence Livermore National Laboratory, University of California, Livermore, California 94550, USA*

This paper reports dynamical mean field calculations for the periodic Anderson model in which the conduction band is coupled to phonons. Motivated in part by recent attention to the role of phonons in the  $\gamma$ - $\alpha$  transition in Ce, this model yields a rich and unexpected phase diagram which is of intrinsic interest. Specifically, above a critical value of the electron-phonon interaction, a first order transition with two coexisting phases develops in the temperature-hybridization plane, which terminates at a second order critical point. The coexisting phases display the familiar Kondo screened and local moment character, yet they also exhibit pronounced polaronic and bipolaronic properties, respectively.

PACS numbers: 71.27.+a, 71.10.Fd, 71.38.-k

The Periodic Anderson Model (PAM) and its impurity variant have played pivotal roles in elucidating the nature of Kondo screening as the techniques of many-body theory have improved [1, 2]. Perhaps its most noted application has been the Kondo Volume Collapse scenario for understanding the unique isostructural  $\gamma$ - $\alpha$  transition in Ce, with its very large 15% volume change [3, 4]. The relative merits of this perspective versus the Mott transition scenario [5] are still under debate, although both focus on critical  $4f$ -electron correlation effects, and the finite temperature predictions are rather similar [6]. The PAM exhibits a smooth crossover from a local moment region with Curie Weiss susceptibility ( $\gamma$ -like) to a region with Kondo screened  $4f$  moments and a paramagnetic susceptibility ( $\alpha$ -like), as a function of increasing hybridization between the  $4f$  and valence electrons [7]. Although the PAM also predicts a first order transition given proper consideration of the Maxwell construction of the free energy versus volume curves [3], it requires modifications like some  $f$ - $f$  hybridization [8] so as to display a first order phase transition with two coexisting phases at the same hybridization in the temperature-hybridization plane.

Over the past decade attention in the Ce literature has shifted to an appreciation that a significant fraction of the total entropy change across the transition may be due to phonons [9–15]. However, studies focusing on the effect of phonons on the PAM are very limited [16–20]. Prior studies either are constrained to ground state calculation or do not explore possible phase transitions in detail. To this end, we are motivated here to consider the PAM with Holstein phonons [21–24]. Since the coupling of phonons to the  $f$ -electrons can lead to loss of local moments via electron condensation, we have chosen to couple the phonons to the conduction electrons in the present work. We find that the electron-phonon interaction above a critical strength induces a first order transition in the temperature-hybridization plane for the PAM-Holstein model. Strikingly the electron-phonon

interaction also creates polaronic behavior in the Kondo screened phase and bipolaronic behavior in the local moment phase. This intriguing phase diagram is explored in the remainder of the present paper.

The Hamiltonian of the PAM-Holstein model is:

$$H = H_0 + H_U + H_{e-ph}, \quad (1)$$

$$H_0 = -t \sum_{\langle i,j \rangle, \sigma} \left( c_{i,\sigma}^\dagger c_{j,\sigma} + c_{j,\sigma}^\dagger c_{i,\sigma} \right) + \epsilon_f \sum_{i,\sigma} f_{i,\sigma}^\dagger f_{i,\sigma} \\ + V \sum_{i,\sigma} \left( c_{i,\sigma}^\dagger f_{i,\sigma} + f_{i,\sigma}^\dagger c_{i,\sigma} \right) + \sum_i \left( \frac{P_i^2}{2m} + \frac{1}{2} k X_i^2 \right)$$

$$H_U = U \sum_i n_{i,\uparrow}^f n_{i,\downarrow}^f$$

$$H_{e-ph} = g \sum_{i,\sigma} n_{i,\sigma}^c X_i,$$

where  $c_{i,\sigma}$ ,  $c_{i,\sigma}^\dagger$  ( $f_{i,\sigma}$ ,  $f_{i,\sigma}^\dagger$ ) are the creation and annihilation operators of the conduction ( $f$ -level) at site  $i$  and spin  $\sigma$ ;  $n_{i,\sigma}^c = c_{i,\sigma}^\dagger c_{i,\sigma}$  and  $n_{i,\sigma}^f = f_{i,\sigma}^\dagger f_{i,\sigma}$  represent the occupation of the  $c$  and  $f$ -electrons, respectively;  $t$  is the nearest neighbor hopping;  $\epsilon_f$ , the on-site energy of the  $f$ -level;  $V$ , the hybridization between conduction and localized electrons; the on-site Hubbard interaction is  $U$ ;  $g$  is the electron-phonon coupling;  $X_i$ , the lattice displacement at site  $i$ , and  $P_i$  its conjugate momentum.

We use the Dynamical Mean Field Theory (DMFT) [25] on a hypercubic lattice in infinite dimensions with Gaussian density of states  $D(\epsilon) = \frac{1}{\sqrt{\pi W}} e^{-\left(\frac{\epsilon}{W}\right)^2}$ . We set the bandwidth  $W = 1.0$  as the unit of energy. In Ce the Fermi energy is about 6000 K and the Debye frequency is 110-160K [9, 15], therefore we set the phonon frequency  $\omega_0 = 0.01$  at 1% of bandwidth. The total electronic density is fixed at  $n = 1.8$  by tuning the chemical potential at each iteration of the DMFT cycle. The Hubbard interaction is  $U = 4.0$ , and we adjust  $\epsilon_f$  so that  $n_f = 1$  at  $T = 0.1$  to ensure that a local moment

is present at large temperatures. Therefore the data we show are for  $n_f \sim 1.0$  and  $n_c \sim 0.8$ . The Continuous Time Quantum Monte Carlo (CTQMC) [26], generalized for electron-phonon coupling [27], is employed as the impurity solver.

Fig. 1 displays the local hybridization factor  $\Gamma = \langle c_0^\dagger f_0 + h.c. \rangle$  (here 0 denotes the impurity site) as a function of  $V$  for  $g^2/2k = 1.0$  and different values of inverse temperature,  $\beta$ . As the temperature decreases, the slope of the  $\Gamma$  vs.  $V$  curve becomes progressively larger, which indicates the system is approaching a critical point. Interestingly, the curves approximately cross for a critical hybridization of  $V_c \sim 0.96$ . The inset of Fig. 1 shows  $\Gamma$  vs.  $V$  at  $g^2/2k = 0.49$ . Notice that for this value of the coupling the slope does not become steeper as the temperature decreases, and the crossing disappears. This indicates that the corresponding susceptibility reaches a plateau as a function of the temperature and the critical behavior is lost. We believe that  $g^2/2k = 0.49$  is a lower bound for the critical value of the electron-phonon coupling.

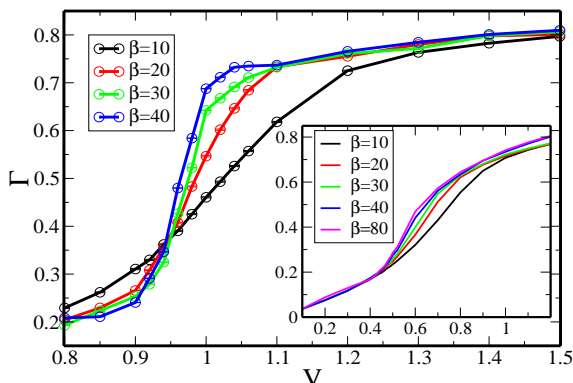


FIG. 1: (color online) Isothermal scan of the hybridization factor  $\Gamma = \langle c_0^\dagger f_0 + h.c. \rangle$  as a function of  $V$  for  $g^2/2k = 1.0$ .  $\Gamma$  increases monotonically with  $V$ . As the temperature decreases,  $\Gamma$  vs.  $V$  becomes steeper with a diverging slope near  $V_c \sim 0.96$ . Inset: The isothermal scan of the hybridization factor  $\Gamma$  as a function of  $V$  at  $g^2/2k = 0.49$ . Notice that the critical behavior has disappeared.

When the temperature is further decreased to  $T = 0.0167$  ( $\beta = 60$ ),  $\Gamma$  vs.  $V$  displays a hysteresis loop as shown in Fig. 2. The red line is obtained by starting at the large  $V$  side ( $V = 1.2$ ), and using the output self-energy to initiate the simulation for the next smaller  $V$ . On the other hand, we obtain the black line by starting at  $V = 0.8$  and using the output self-energy as the input for the next larger value of  $V$ . The coexistence of two solutions for the same value of  $V$  at  $T = 0.0167$  is a direct evidence of a first order phase transition. The absence of such a hysteresis at higher temperatures indicates that the first order transition ends at a second order terminus ( $V_c, T_c$ ).

For the same parameters,  $V = 0.96$ ,  $g^2/2k = 1.0$ ,  $\omega_0 = 0.01$ , and  $U = 4.0$ , we also perform a series of isothermal

scans on the chemical potential to study the relationship between the total electron density  $n = n_c + n_f$  and the chemical potential  $\mu$ . As long as the temperature is not below  $T = 0.0167$ , the compressibility  $\frac{dn}{d\mu}$  shows no tendency to diverge. This indicates the phase transition here is not compressibility driven.

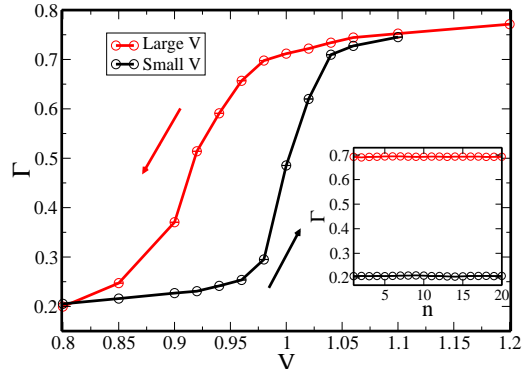


FIG. 2: (color online) Hysteresis of  $\Gamma$  vs.  $V$  for  $T = 0.0167$ ,  $g^2/2k = 1.0$ . The black line represents the small  $V$  branch of the hysteresis for which the self-energy of the previous simulation is used to initiate the calculation for the next larger value of  $V$ . While the red line represents the large  $V$  branch where starting with  $V = 1.2$  we use the output of the previous simulation to initiate the computation at the next lower value of  $V$ . Inset:  $\Gamma$  as a function of the DMFT iteration number  $n$  for  $V = 0.96$ ,  $T = 0.0167$ . The black (red) symbols represent the small (large)  $V$  branches.

In Fig. 3 we show the temperature times the local  $f$ -orbital spin susceptibility,  $T \cdot \chi_s^{ff}$ , versus temperature. As  $T$  approaches zero  $T \cdot \chi_s^{ff}$  is roughly constant for  $V = 0.8$ , while it goes to zero for  $V = 1.2$ . This indicates that at  $V = 0.8$  the  $f$ -electrons display a robust local moment and paramagnetic local susceptibility with  $1/T$  dependence, while at  $V = 1.2$  the  $f$  local moments are quenched. The inset of Fig. 3 shows the  $f$ -orbital density of states (DOS) at  $T = 0.01$ . Notice that at  $V = 0.8$  there is a gap across the Fermi level, while at  $V = 1.2$  a Kondo resonance peak appears. The screening of the local moment in the large  $V$  region is a consequence of the singlet formation between  $c$  and  $f$ -electrons.

The main panel of Fig. 4 shows the occupancy distribution histogram of the  $c$ -electrons,  $P(n_c)$ , at  $T = 0.0167$ .  $P(n_c)$  has been used to illustrate bipolaron formation [27]. At  $V = 0.8$  the  $c$ -orbital electrons are in a bipolaronic state, which is characterized by the oscillation between zero and double occupancy. While for  $V = 1.2$ , the  $c$ -electrons are in a polaronic state, where the occupancy oscillates between zero and one. For the PAM, without electron-phonon coupling, the structure of  $P(n_c)$  is totally different. Here there is only one peak at roughly the  $c$ -electron filling  $n_c = 0.8$ , and  $P(n_c)$  quickly decays to zero for  $n_c$  away from this filling. In the inset, the quasi-particle fraction  $Z$  is plotted as a function of temperature. The quasi-particle fraction is calculated

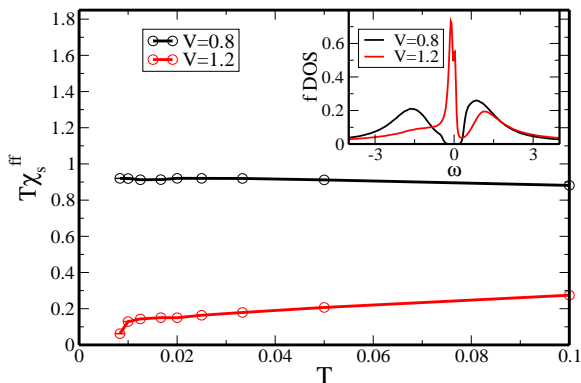


FIG. 3: (color online) Temperature times the local  $f$ -orbital spin susceptibility,  $T \cdot \chi_s^{ff}$ , as a function of temperature for  $g^2/2k = 1.0$ . For  $V = 0.8$  (black line),  $T \cdot \chi_s^{ff}$  approaches a constant value as  $T \rightarrow 0$  indicating an unscreened moment. For  $V = 1.2$  (red line),  $T \cdot \chi_s^{ff}$  converges to zero indicating the local moment is screened. Inset: The  $f$ -electron DOS at  $T = 0.01$ . The Kondo peak found for  $V = 1.2$  (red line), but absent for  $V = 0.8$  (black line) is consistent with the screening and unscreening scenarios in the main panel.

for the lower quasiparticle band at the Fermi level using a generalization of the single band formulation [28]. The main component of this approach is to make the replacement  $\frac{d\text{Re}\Sigma(\omega)}{d\omega}|_{\omega=0} \approx \frac{\text{Im}\Sigma(i\pi T)}{\pi T}$ , which becomes exact at zero temperature. As  $T \rightarrow 0$ ,  $Z$  goes to zero for  $V = 0.8$  indicating non-Fermi liquid behavior, while it converges to a finite value for  $V = 1.2$ , the signature of Fermi liquid formation.

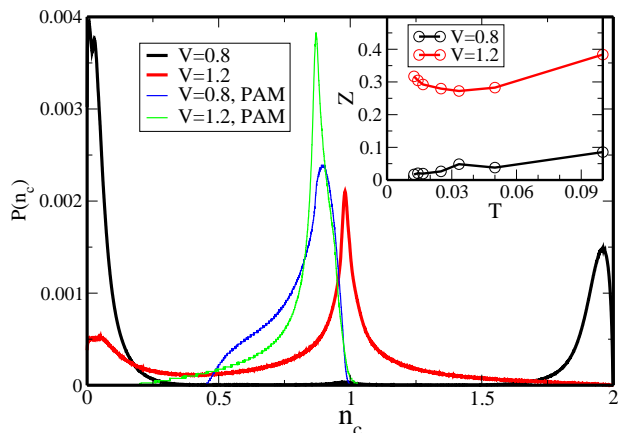


FIG. 4: (color online) Occupancy distribution histogram of  $c$ -orbital  $P(n_c)$  for  $V = 0.8$  (black line) and  $1.2$  (red line),  $T = 0.0167$  and  $g^2/2k = 1.0$ . For comparison,  $P(n_c)$  of the PAM without electron-phonon coupling is plotted as well:  $V = 0.8$  (blue line) and  $V = 1.2$  (green line). Inset: the quasiparticle  $Z$  factor as a function of temperature for  $V = 0.8$  (black line) and  $1.2$  (red line).

We find that this Kondo singlet to local moment phase transition remains for a large range of parameters, like adjusting the total filling to  $n = 1.6$ , changing the Hubbard interaction to  $U = 3.8$  and increasing the phonon frequency to  $\omega_0 = 0.02$  and  $\omega_0 = 0.05$ , while keeping  $g^2/2k$  fixed. For these different parameters, we find that

the isothermal  $\Gamma$  vs.  $V$  curves still cross and their slopes diverge at a critical value of the hybridization,  $V_c$ , as the temperature is decreased. We also find that  $V_c$  changes roughly linearly with  $g^2/2k$ .

In Fig. 5(a) the time integrated local  $f$ -orbital spin-spin correlation function,  $\chi_s^{ff}$ , is plotted as a function of temperature for  $V = 1.1, 1.2$  and  $1.3$ . We identify the Kondo scale  $T_K$  as the energy where  $\chi_s^{ff}$  falls to around half of its low temperature value. We find that  $T_K$  changes very little as  $V$  increases, so the line  $V$  vs.  $T_K$  should have a large slope. Fig. 5(b) shows the time integrated local  $c$ -orbital spin-spin correlation function,  $\chi_s^{cc}$  vs.  $V$ , at different temperatures, where large values reflect the  $c$ -electron spin degeneracy in the polaronic state in contrast to the small susceptibility for the spinless bipolarons. For  $V < 0.96$  the curves almost overlap for all  $T < 0.1$ . In fact, the corresponding  $c$ -electron occupancy histograms (not shown) show an obvious bipolaronic double peak feature even at relatively high temperatures like  $T = 0.1$ . If we define  $T^*$  as the energy where bipolaron formation begins, then the line  $T^*$  vs.  $V$  must be nearly horizontal.

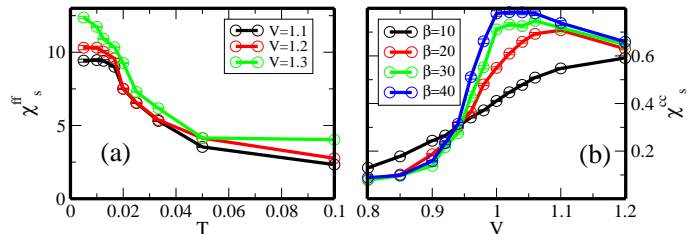


FIG. 5: (color online) Panel (a) shows the  $f$ -orbital time integrated local spin-spin correlation,  $\chi_s^{ff}$ , as a function of temperature for  $V = 1.1, 1.2$  and  $1.3$ . Panel (b) shows the  $c$ -orbital time integrated local spin-spin correlation function,  $\chi_s^{cc}$ , as a function of  $V$  for different temperatures.

We have also calculated the renormalized phonon frequency. At  $T = 0.025$  it is roughly constant for hybridization  $V > 0.96$ ; however, it drops precipitously for  $V < 0.96$ , decreasing by half when  $V = 0.8$ . This behavior softens with increasing temperature, e.g., a more gradual decrease begins for  $V < 1.2$  at  $T = 0.1$ . This indicates an important temperature dependence of the phonons properties. Indeed the analysis in [13] for Ce found that the temperature dependence of the phonons was a critical factor for obtaining a significant phonon contribution to the entropy change across the  $\gamma$ - $\alpha$  transition [9–15].

Fig. 6 is a schematic summary of our findings. Two phases, local moment-bipolaron and Kondo singlet-polaron, are separated by a first order transition line, which terminates at a second order critical point  $(V_c, T_c)$ . The positive slope of the  $V$  vs.  $T$  first order transition line is a consequence of a Clausius-Clapeyron-like relation where hybridization  $V$  is the intensive analog of pressure. There is no broken symmetry between these two phases

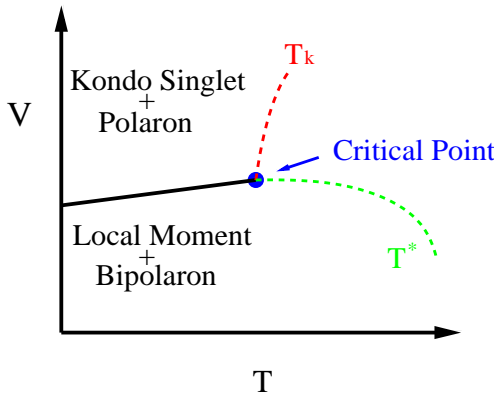


FIG. 6: (color online) Schematic  $V$  vs.  $T$  phase diagram. The solid black line represents the first order phase transition which separate the local moment-bipolaron phase for small  $V$  from the Kondo singlet-polaron phase for large  $V$ . This first order phase terminates at a second order critical point. The red dashed line coming out of the critical point represents the Kondo scale  $T_K$  and the green dashed line the bipolaron energy scale  $T^*$ .

as we can move adiabatically from one to another by wandering around the critical point. Both phases are destroyed by increasing the temperature. In order to have such a first order phase transition, the electron-phonon coupling on the  $c$ -band must be larger than a certain critical value. The fact that the critical temperature is a function of electron-phonon coupling implies that the critical point touches zero temperature at some  $g_c$ , where the first order phase transition becomes a quantum phase transition tuned by  $V$ .

In conclusion, when the conduction band of the periodic Anderson model is coupled to phonons, one obtains a rich and unexpected phase diagram. Above a critical strength of the electron-phonon coupling a first order transition with two coexisting phases develops in the temperature-hybridization plane. This transition terminates at a second order critical point. These coexisting phases correspond to the familiar Kondo screened and local moment regions of the PAM, yet, they additionally exhibit pronounced polaronic and bipolaronic behavior, respectively. While the PAM and its impurity variant have been paradigms for the  $\gamma$ - $\alpha$  transition in Ce, additional electronic bands not considered here might be needed in a generalization of the present PAM-Holstein model to more completely explain the volume collapse. Nonetheless, the present simple model illustrates a fundamental principle relevant to the electron-phonon interaction in Ce. The Kondo temperature, which measures the critical energy scale of hybridization between  $4f$  and valence electrons, has a roughly exponential volume dependence leading to an order of magnitude increase from  $\gamma$ - to  $\alpha$ -Ce [3, 4]. This scale is comparable to that of the

lattice vibrations (Debye temperature) [15] only in the  $\gamma$  phase of Ce, and so it is no accident that the present work finds the most dramatic manifestations of the electron-phonon interaction, a bipolaronic state with significant phonon softening, in this local moment region.

We thank Thomas Pruschke for valuable discussions. This work is supported by NSF OISE-0952300 (PZ, PR, JM), DOE SciDAC grant DE-FC02-06ER25792 (KMT, MJ), and at LLNL by DOE contract DE-AC52-07NA27344 (AM). This work used the Extreme Science and Engineering Discovery Environment (XSEDE), which is supported by National Science Foundation grant number DMR100007.

- 
- [1] A.C. Hewson, *The Kondo Problem to Heavy Fermions*, Cambridge University Press, New York, N.Y., (1993).
  - [2] M. Jarrell, H. Akhlaghpour, and T. Pruschke, Phys. Rev. Lett. **70**, 1670 (1993).
  - [3] J. W. Allen and R. M. Martin, Phys. Rev. Lett. **49**, 1106 (1982); M. Lavagna, C. Lacroix, and M. Cyrot, Phys. Lett. **90A**, 210 (1982).
  - [4] J. W. Allen and L. Z. Liu, Phys. Rev. B **46**, 5047 (1992).
  - [5] B. Johansson, Philos. Mag. **30**, 469 (1974).
  - [6] K. Held, C. Huscroft, R. T. Scalettar, and A. K. McMahan, Phys. Rev. Lett. **85**, 373 (2000).
  - [7] C. Huscroft, A.K. McMahan, and R.T. Scalettar, Phys. Rev. Lett. **82**, 2342 (1999).
  - [8] L. de' Medici, A. Georges, G. Kotliar, and S. Biermann, Phys. Rev. Lett. **95**, 066402 (2005).
  - [9] M. E. Manley, *et al.*, Phys. Rev. B **67**, 014103 (2003).
  - [10] I.-K. Jeong *et al.*, Phys. Rev. Lett. **92**, 105702 (2004).
  - [11] F. Decremps, D. Antonangeli, B. Amadon and G. Schermer, Phys. Rev. B **80**, 132103 (2009).
  - [12] D. Antonangeli *et al.*, High Press. Res. **30**, 151 (2010).
  - [13] M. J. Lipp, *et al.*, Phys. Rev. Lett. **101**, 165703 (2008).
  - [14] B. Johansson, *et al.*, Phys. Rev. Lett. **102**, 189601 (2009).
  - [15] M. Krisch, *et al.*, Proc. Natl. Acad. Sci. **108**, 9342 (2011).
  - [16] K. Mitsumoto, Y. Ōno, Physica C **426**, 330 (2005).
  - [17] Takashi Hotta, J. Phys. Soc. Jpn. **76**, 084702 (2007).
  - [18] R. Nourafkan, and N. Nafari, Phys. Rev. B. **79**, 075122 (2009).
  - [19] M. Raczkowski, *et al.*, Phys. Rev. B. **81**, 054444 (2010).
  - [20] O. Bodensiek, *et al.*, J. Phys.: Condens. Matter **23**, 094212 (2011).
  - [21] T. Holstein, Ann. Phys. (N.Y.) **8**, 325; **8**, 343 (1959).
  - [22] J. K. Freericks, M. Jarrell, and D. J. Scalapino, Phys. Rev. B **48**, 6302 (1993).
  - [23] W. Koller, D. Meyer, Y. Ōno, and A. Hewson, Europhys. Lett. **66**, 559 (2004).
  - [24] M. Capone, P. Carta, S. Ciuchi, Phys. Rev. B **74**, 045106 (2006).
  - [25] A. Georges, G. Kotliar, W. Krauth and M. J. Rozenberg, Rev. Mod. Phys. **68**, 13 (1996).
  - [26] A. N. Rubtsov, V. V. Savkin, and A. I. Lichtenstein, Phys. Rev. B **72**, 035122 (2005).
  - [27] F.F. Assaad, T. Lang, Phys. Rev. B **76**, 035116 (2007).
  - [28] D.W. Hess and J.W. Serene, J. Phys. Chem. Solids **52**, 1385 (1991).